Conf-920375--23

Evaluation of Aging Degradation of Structural Components*

O. K. Chopra and W. J. Shack

Materials and Components Technology Division
Argonne National Laboratory
9700 South Cass Avenue
Argonne, Illinois 60439 USA

ANL/CP--75790

DE92 014849

March 1992

Presented at NRC Aging Research Information Conference, March 24–27, 1992, Rockville, MD.

*Work supported by the Office of Nuclear Regulatory Research, U.S. Nuclear Regulatory Commission, FIN No. A22562; Project Manager: E. Woolridge.

Evaluation of Aging Degradation of Structural Components*

O. K. Chopra and W. J. Shack

Materials and Components Technology Division
Argonne National Laboratory
9700 South Cass Avenue
Argonne, Illinois 60439 USA

Abstract

Irradiation embrittlement of the neutron shield tank (NST) A212 Grade B steel from the Shippingport reactor, as well as thermal embrittlement of CF-8 cast stainless steel components from the Shippingport and KRB reactors, has been characterized. Increases in Charpy transition temperature (CTT), yield stress, and hardness of the NST material in the low-temperature low-flux environment are consistent with the test reactor data for irradiations at <232°C. The shift in CTT is not as severe as that observed in surveillance samples from the High Flux Isotope Reactor (HFIR); however, it shows very good agreement with the results for HFIR A212-B steel irradiated in the Oak Ridge Research Reactor. The results indicate that fluence rate has no effect on radiation embrittlement at rates as low as 2×10^8 n/cm^2·s at the low operating temperature of the Shippingport NST, i.e., 55°C. This suggest that radiation damage in Shippingport NST and HFIR surveillance samples may be different because of the neutron spectra and/or Cu and Ni content of the two materials. Cast stainless steel components show relatively modest decreases in fracture toughness and Charpy-impact properties and a small increase in tensile strength. Correlations for estimating mechanical properties of cast stainless steels predict accurate or slightly conservative values for Charpy-impact energy, tensile flow stress, fracture toughness J-R curve, and J_{IC} of the materials. The kinetics of thermal embrittlement and degree of embrittlement at saturation, i.e., the minimum impact energy achieved after long-term aging, were established from materials that were aged further in the laboratory. The results were consistent with the estimates. The correlations successfully predict the mechanical properties of the Ringhals 2 reactor hot- and crossover-leg elbows (CF-8M steel) after service of ≈15 y.

1 Introduction

Structural materials exposed to reactor environments undergo microstructural changes that can influence mechanical and corrosion properties and thus compromise the integrity of structure components. Although aging phenomena such as the embrittlement of cast stainless steels, low-temperature sensitization of austenitic stainless steels, and radiation embrittlement of pressure vessel steels have been studied in the laboratory, most of the studies are based on simulations of actual reactor conditions. Service-aged components from decommissioned and operating reactors offer a unique opportunity to validate the laboratory studies, thereby providing a sound basis for evaluating structural integrity near the end of the projected life of the plant. This paper presents an evaluation of irradiation embrittlement of the neutron shield tank (NST) material from the Shippingport reactor, as well as of thermal embrittlement of cast stainless steels from the Shippingport and KRB reactors. The results are compared with estimates based on laboratory studies.

*Work supported by the Office of Nuclear Regulatory Research, U.S. Nuclear Regulatory Commission, FIN No. A22562; Project Manager: E. Woolridge.

2 Neutron Shield Tank Studies

2.1 Background

Data on surveillance specimens from the high-flux isotope reactor (HFIR) at Oak Ridge National Laboratory showed a very high degree of embrittlement in A212 Grade B, A350 Grade LF3, and A105 Grade II steels[1,2] relative to that of similar materials irradiated at low temperatures in test reactors.[3] The HFIR surveillance specimens were exposed for ≈17 effective-full-power years (efpy) at 50°C and a flux (E >1 MeV) of 10^8–10^9 n/cm^2·s to fluences of 10^{17}–10^{18} n/cm^2. The fast-neutron flux for the HFIR surveillance samples was several orders of magnitude lower than that in test reactors (10^{13} n/cm^2·s). One explanation of the difference between HFIR and test reactor data is that the degree of embrittlement per unit of fast fluence increases at low neutron flux, i.e., the difference is due to a fluence-rate effect.[1] The possible effects of fluence rate were validated by comparative tests on HFIR A212-B steel irradiated in the Oak Ridge Research Reactor (ORR) at a flux of ≈10^{13} n/cm^2·s.[1,2] The results indicated that an order of magnitude greater fluence is needed in the ORR to produce the same shift in Charpy transition temperature (CTT) that was observed in HFIR A212-B surveillance samples. Current Nuclear Regulatory Commission guidelines for the assessment of embrittlement of pressure vessel support structures of commercial LWRs do not consider the contributions of fluence rate. HFIR surveillance data raise the possibility that the guidelines may not be sufficiently conservative.[4]

To resolve this issue, the irradiation embrittlement of NST from the decommissioned Shippingport reactor has been characterized. The NST support for the reactor pressure vessel is a skirt-mounted, annular, water-filled tank that consists of two concentric shells extending above and below the reactor core. It is exposed to reactor-core beltline neutrons. Water is circulated through the tank for cooling and shielding. Shippingport NST operated at 55°C and was fabricated from rolled A212 Grade B firebox steel similar to that used for the HFIR pressure vessel. Eight ≈155-mm disc samples of the base metal and three weld samples were obtained from the inner wall, along with corresponding samples of the outer wall. A detailed description of the sampling and metallurgical characterization of the materials has been presented elsewhere.[5,6] The inner wall of the NST was exposed to a total maximum fluence of ≈6 x 10^{17} n/cm^2 (E >1 MeV) over a life of 9.25 efpy. This corresponds to a fast-neutron flux of ≈2 x 10^9 n/cm^2·s. The temperature, fast fluence, and fast flux for the Shippingport NST were comparable to those for the HFIR surveillance samples. Material from the outer wall, which was protected by ≈0.9 m of water and hence had a fluence six orders of magnitude lower than that of the irradiated wall, was used to obtain baseline data for nonirradiated material.

2.2 Irradiation Embrittlement of Shippingport NST

Irradiation embrittlement was characterized by Charpy-impact and tensile tests and by hardness measurements; the results have been presented earlier.[5,6] Specimens were obtained in the longitudinal (LT) and transverse (TL) orientations* from three 10-mm-wide regions (inner, center, and outer) across the thickness of the NST wall. Total fluence varied with the axial and azimuthal position of the NST samples. Also, the fluence for specimens from the outer-10-mm region were estimated to be a factor of 1.5 lower than those for specimens from inner-10-mm region. The estimated values of fluence and displacement

*The first letter designates the direction normal to the plane of the crack, and the second letter represents the direction of crack propagation. L = longitudinal or rolling direction and T = transverse direction.

Table 1. Summary of Charpy-impact and tensile results for the Shippingport NST

Location[a]	Flux (E > 1 Mev), n/cm^2·s	Fluence (E > 1 Mev), n/cm^2	dpa	41-J CTT, °C (°F)	41-J ΔCTT, °C (°F)	20.4-J CTT, °C (°F)	20.4-J ΔCTT, °C (°F)	Yield Stress, MPa	ΔYield, MPa
	-	-	-	31 (88)	-	16 (61)	-	294	-
2, 8 Outer	8.90 x 10^8	2.67 x 10^{17}	7.10 x 10^{-4}	51 (124)	20 (36)	39 (102)	23 (41)	345[b]	51
3, 9 Outer	1.33 x 10^9	4.00 x 10^{17}	1.07 x 10^{-3}	51 (124)	20 (36)	39 (102)	23 (41)	345[b]	51
2, 8 Inner	1.33 x 10^9	4.00 x 10^{17}	1.07 x 10^{-3}	58 (136)	27 (48)	44 (111)	28 (50)	345[b]	51
3, 9 Inner	2.00 x 10^9	6.00 x 10^{17}	1.60 x 10^{-3}	58 (136)	27 (48)	44 (111)	28 (50)	345[b]	51

[a]Samples from inner- and outer-10-mm region of the irradiated inner wall of the NST and nonirradiated samples from the shielded outer wall.
[b]Average value at all fluence levels.

per atom (dpa), as well as measured Charpy-impact and tensile properties, of LT specimens from various locations of the NST are given in Table 1.

The results for the essentially nonirradiated outer wall showed no effect of sample location; there was little or no variation in the transition curves with vertical or azimuthal position. However, the NST material is significantly weaker in TL than in the LT orientation. The CTT and upper-shelf energy (USE), respectively, are 16°C and 102 J/cm^2 for LT, and 20°C and 67 J/cm^2 for TL specimens. The differences in impact strength for the two orientations are attributed primarily to differences in the distribution of inclusions along the crack plane. The plane of the crack for the TL orientation contains elongated inclusions.

The irradiated specimens showed a higher CTT and lower USE relative to those from the outer wall. Some effects of position through the thickness of the wall are observed for LT specimens, as shown in Fig. 1. The values of CTT are 39°C for specimens from the outer-10-mm region and 44°C for inner-10-mm region, a shift of ≈23 and 28°C for the outer and inner regions, respectively. The USE for both regions is ≈77 J/cm^2, a decrease of 25 J/cm^2. The shift in CTT of the TL specimens is also 23°C. However, the USE is lower, i.e., 52 J/cm^2.

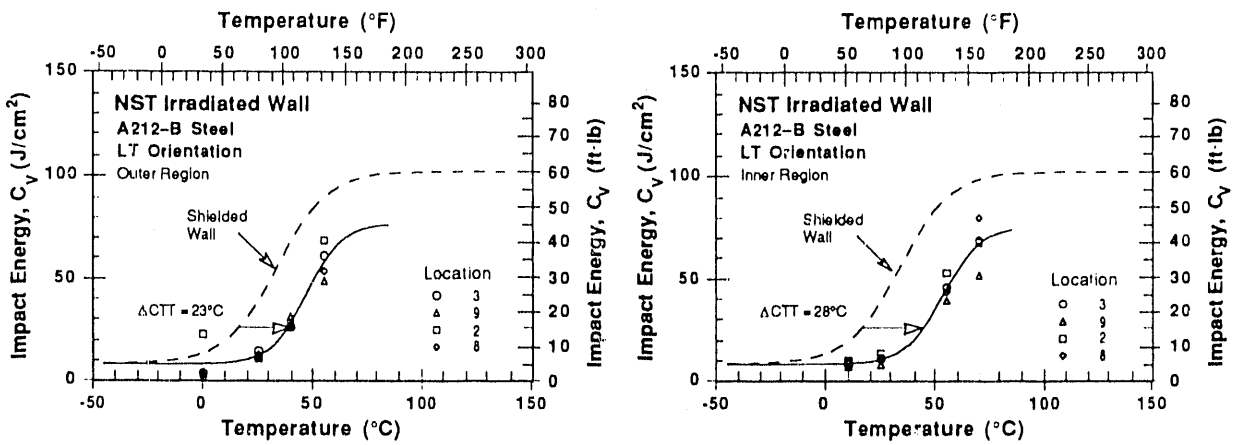

Figure 1. Best-fit Charpy transition curves for (a) outer- and (b) inner-region LT specimens from the irradiated wall of the Shippingport NST

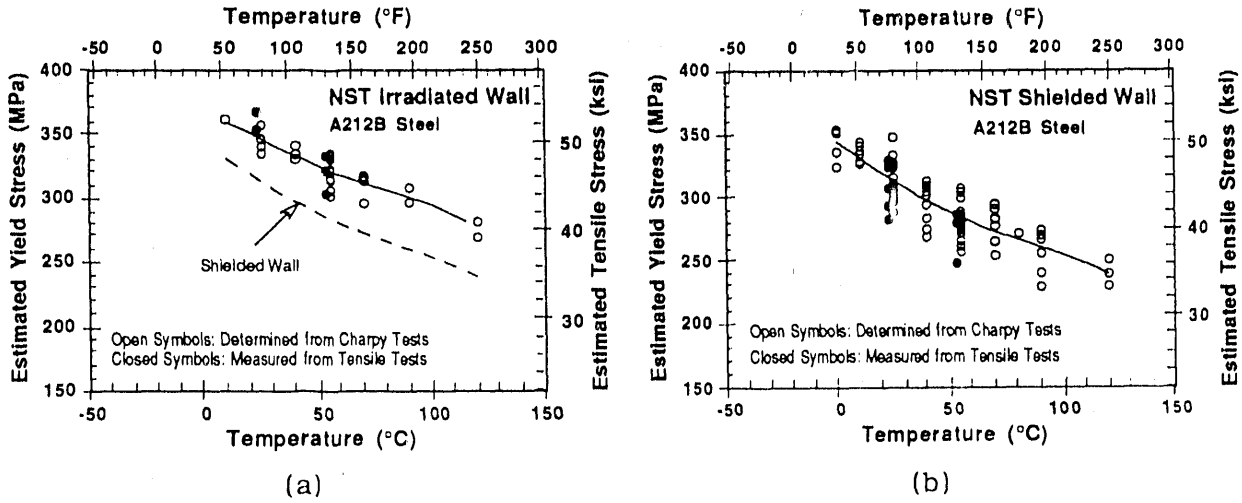

Figure 2. Yield stress estimated from Charpy-impact tests and measured from tensile tests for (a) irradiated and (b) shielded walls of the Shippingport NST

Tensile tests were conducted at room temperature and at 55°C on LT specimens from several locations of the irradiated and shielded walls of the NST and from three regions across the thickness of the wall. Irradiation increased the tensile strength of the NST material. The increases in yield and ultimate stress were, respectively, ≈51 and 20 MPa at room temperature, and ≈38 and 18 MPa at 55°C. The tensile properties of the NST material were also estimated from the Charpy-impact data. Yield stresses estimated from Charpy-impact tests and those obtained from tensile tests for material from the irradiated inner wall and shielded outer wall are shown in Fig. 2. The results show the expected decrease in yield stress with an increase in test temperature. Irradiation increases the yield stress at all test temperatures.

The tensile data for the Shippingport NST show very good agreement with the correlations between the increases in CTT and yield stress that have been developed for pressure vessel steel.[7,8] The CTT shift (°C) and increase in yield stress (MPa) is expressed as

$$\Delta CTT = C\Delta\sigma_y, \quad (1)$$

where C is ≈0.5°C/MPa for plate material, and 0.65°C/MPa for welds. The shift in the CTT of both LT and TL specimens is 23°C (28°C for LT specimens from inner regions), and the increase in yield stress is 51 MPa.

Annealing studies indicate complete recovery from embrittlement after 1 h at 400°C. Hardness of the irradiated wall decreased by 9–14 DPH. Correlations between increases in hardness and yield stress from radiation hardening of pressure vessel steels indicate that the increase in yield stress (MPa) is 3.5 times the increase in hardness (DPH).[7,8] Based on tensile and Charpy-impact data, the increases in hardness of the irradiated NST material are in fair agreement with the estimation.

2.3 Low-Temperature Irradiation

The shift in CTT of the Shippingport NST is not as severe as that observed in HFIR surveillance specimens. However, the actual value of the CTT is higher than that for the HFIR specimens. Except for minor differences in Cu and Ni contents, elemental compositions of the A212-B steels from the HFIR pressure vessel and from the Shippingport NST

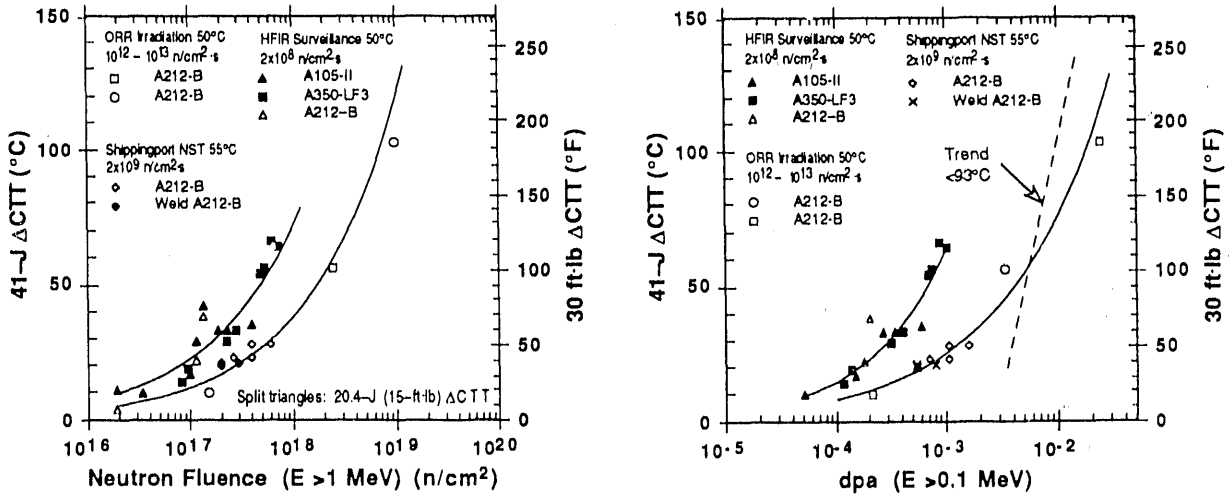

(a) (b)

Figure 3. Shifts in CTT with (a) neutron fluence and (b) dpa for the Shippingport NST material, HFIR surveillance samples, and HFIR A212-B irradiated in the ORR. The dashed line represents the trend curve for data from test reactors.

are comparable. The differences in the transition curves of the nonirradiated A212-B steels are most likely due to microstructural factors, e.g., amount and distribution of inclusions.

The shifts in CTT of the material from the Shippingport NST, HFIR surveillance samples, and HFIR A212-B steel irradiated in the ORR are plotted as a function of neutron exposure in Fig. 3a. The results for the Shippingport NST material are consistent with those from ORR-irradiated steel. The HFIR surveillance data follow a different trend; for a given fluence, the shifts in CTT are greater than those for the Shippingport NST material or the ORR-irradiated samples.

To account for differences in the spectra of the various irradiation facilities, the increase in CTT for HFIR surveillance steels, ORR-irradiated samples, and the Shippingport NST, as well as the trend curve for test reactor data* at <93°C, are plotted in Fig. 3b as a function of dpa for E >0.1 MeV rather than fluence. The difference still exists between HFIR surveillance data and results from ORR irradiation, the Shippingport NST, or test reactors.

Irradiation temperature is an important factor in radiation damage, particularly in the temperature range of operation of power reactors. At temperatures >232°C, progressively lower embrittlement is observed with increasing temperature.[9-11] However, relatively little or no temperature effect is observed at irradiation temperatures <232°C. In Fig. 4a, the results for the Shippingport NST and for samples irradiated in the ORR are compared with data from test reactors[3,10-16] and from the Army reactors surveillance program.[17,18] The shifts in CTT for the NST A212-B and HFIR A212-B irradiated in the ORR are consistent with these results and represent the tail of the trend band that describes the increase in CTT of various steels irradiated at <232°C.

*From Ref. 4, where the test reactor trend curve was obtained assuming that the calculated spectrum for ORR was appropriate for test reactor data.

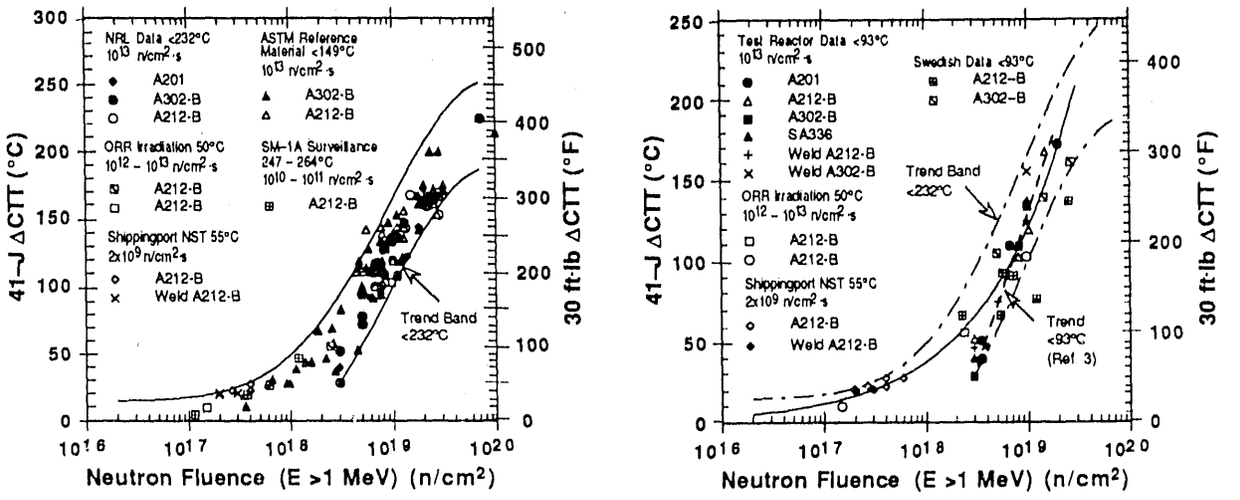

Figure 4. Comparison of CTT shifts for the Shippingport NST and ORR-irradiated specimens with test reactor data for irradiations at (a) <264°C and (b) <93°C

Swedish data[19] on the effect of irradiation temperature on embrittlement of ferritic steels (including A212-B steel) indicate that embrittlement is relatively insensitive to temperature between 110 and 232°C and decreases at lower and higher temperatures. The data from irradiation of various steels and welds[3,17] at <93°C fall between the center and lower-bound curve of the <232°C trend band (Fig. 4b). Swedish data from irradiations at 110–230°C follow the upper bound of the trend band.

The data in Fig. 4a indicate that variations in chemical composition of steel, e.g., Cu or Ni contents, have little or no effect on irradiation embrittlement at <232°C. For example, the increases in CTT for ASTM reference A212-B and A302-B steels irradiated at <149°C are comparable. Compositional effects are observed for these steels when they are irradiated in the same facilities at higher temperatures.[16]

Surveillance data for Army reactors indicate no significant difference in embrittlement between A212-B and A350 steels.[12,17,18] The results for A350 steels in Army reactors, are within the trend band for irradiations at <232°C, although they are close to the upper-bound curve. HFIR surveillance data for A350-LF3 and A105-II steels do not follow the trend for A350 Army reactor steels; they show greater embrittlement than the <232°C trend band. These results suggest that the greater embrittlement of HFIR surveillance samples relative to the Shippingport NST is primarily due to factors other than material and compositional differences.

The greater embrittlement of HFIR surveillance samples relative to that of specimens irradiated in the ORR and test reactors has been evaluated on the basis of a fluence-rate effect.[4] The rate effect was established from specimens irradiated at fluence rates $\leq 1 \times 10^{10}$ n/cm^2·s. HFIR surveillance data for the A350-LF3 and A212-B steels, corresponding to flux values of 2.4×10^8 and 1.2×10^9 n/cm^2·s, respectively, were used to obtain plots of dpa vs. dpa rate for specific CTT shifts. The fluence rate for the Shippingport NST is comparable to the rates for HFIR A350-LF3 or A105-II steels, i.e., $\approx 1 \times 10^9$ n/cm^2·s. If fluence rate has a large effect on the CTT shifts, the values for the Shippingport NST should be close to those for A350-LF3 and A105-II steels. From Ref. 4, the predicted increase in CTT of 45–60°C

for the Shippingport NST is higher by a factor of ≈2 than the measured shifts in CTT. The results for the Shippingport NST indicate that fluence rate has no effect on the shift in CTT at values as low as 2×10^9 n/cm^2·s. The greater embrittlement of HFIR surveillance samples is most likely due to spectral effects.

The HFIR spectrum is highly thermalized, with thermal neutrons accounting for 96% of the total flux in the surveillance position. In the Shippingport reactor and most test reactors of interest, the thermal neutron flux is a much smaller fraction of the total flux. Thermal neutrons cannot cause damage by elastic scattering since the minimum neutron energy required to displace an atom is above 0.5 keV. Damage associated with thermal neutrons is caused by recoil events resulting from neutron capture, i.e., from the (n, γ) reaction and, for some cases, the (n, α) reaction. Radiation effects depend on the fraction of point defects that survive rather than on the production of defects. Slow neutrons in an energy range of <0.1 MeV increase the available point defects per unit displacement, resulting in enhanced cluster formation and embrittlement. Contributions of slow neutrons are not accounted for in conventional methods for assessing damage in terms of fast-neutron fluence (E >1 MeV) or dpa (E >0.1 MeV). Alternative measures of damage assessment must be considered for cases of a softened neutron spectrum such as that of the HFIR.

3 Aging Degradation of Cast Stainless Steels

3.1 Background

Cast duplex stainless steels used in light water reactor (LWR) systems for primary pressure-boundary components such as valve bodies, pump casings, and primary coolant piping are susceptible to thermal embrittlement after extended service at reactor operating temperatures, i.e., 280–320°C. Aging of cast stainless steels at these temperatures leads to increased hardness and tensile strength and decreased ductility, impact strength, and fracture toughness. Investigations at Argonne National Laboratory and elsewhere have shown that thermal embrittlement of cast stainless steels can occur during the reactor design life of 40 y.[20-22] A procedure and correlations have been developed for estimating fracture toughness, tensile, and Charpy-impact properties of cast stainless steel components during thermal aging.[23,24] Because the embrittlement mechanisms and kinetics are complex, microstructural studies and mechanical testing of actual component materials that have completed long in-reactor service are necessary to ensure that the mechanisms observed in accelerated aging experiments are the same as those occurring in reactors. The mechanical-property degradation of cast stainless steel components from the Shippingport reactor have been characterized and the results are compared with estimates from accelerated laboratory aging studies.

Cast stainless steel materials were obtained from four cold-leg check valves, two hot-leg main shutoff valves, and two pump volutes of the Shippingport reactor. One of the volutes is a "spare" that had seen service only during the first core loading, whereas the other was in service for the entire life of the plant. The actual time-at-temperature for the materials was ≈13 y at ≈281°C for the hot-leg components and ≈264°C for the cold-leg components. The components were in a hot stand-by condition of ≈204°C for an additional ≈2 y. Service-aged material was also obtained from the recirculating-pump cover assembly of the KRB reactor, which was in service in Gundremmingen, Germany, for ≈8 y at 284°C.

The chemical composition, hardness, and ferrite content and distribution of the cast materials are given in Table 2. All materials are CF-8 grade cast stainless steel with ferrite contents in the range of 2–16% for the Shippingport components and 34% for the KRB

Table 2. Chemical composition, ferrite morphology, and hardness of cast stainless steel components from the Shippingport, KRB, and Ringhals reactors.

Mater. ID[a]	Composition, wt.%										Ferrite		Ferrite Spacing, μm	Hardness, R_B
	C	N	Si	Mn	P	S	Ni	Cr	Mo	Cu	Calc., %	Meas., %		
Cold Leg Check Valve[b]														
CA4	0.056	0.041	1.45	1.10	0.018	0.009	8.84	20.26	0.01	0.07	10.8	10.9	157	79.8
CA7	0.058	0.041	1.43	1.09	0.018	0.009	8.72	20.22	0.01	0.07	10.9	10.0	148	78.6
CB7	0.052	0.053	1.36	1.07	0.018	0.011	8.85	19.12	0.02	0.06	5.9	3.2	296	75.0
Hot Leg Main Shutoff Valve[b]														
MA1	0.052	0.049	0.22	0.72	0.039	0.013	10.50	20.74	0.24	0.13	5.2	9.5	217	76.9
MA9	0.052	0.051	0.24	0.72	0.041	0.011	10.54	20.78	0.24	0.13	5.1	10.0	245	77.6
MB2	0.042	0.073	0.51	0.72	0.043	0.017	10.77	19.74	0.19	0.12	2.6	1.9	–	74.2
Pump Volute[c]														
VR	0.046	0.049	1.14	0.50	0.027	0.017	9.56	20.79	0.04	0.07	9.8	16.2	181	82.9
PV	0.108	0.027	0.89	1.11	0.032	0.008	9.30	19.83	0.38	0.25	4.1	13.0	–	–
KRB Pump Cover Plate[d]														
KRB	0.062	0.038	1.17	0.31	–	–	8.03	21.99	0.17	–	27.7	34.0	–	–
Ringhals Reactor Elbows[e]														
H	0.037	0.044	1.03	0.77	0.022	0.008	10.60	20.00	2.09	0.17	13.0	20.1	–	–
C	0.039	0.037	1.11	0.82	0.020	0.012	10.50	19.60	2.08	0.08	12.3	19.8	–	–

[a] For the valves, the second digit indicates the loop where the valve was located and the number designates the segment of the component from which the material was removed (segments 1, 2, and 7 are from the top of the valve, segment 4 is from the bottom, and segment 9 is from a cooler region).
[b] In service for ≈13 y at 264°C for cold leg and at 281°C for hot leg.
[c] Spare pump volute VR in service only during initial core loading and PV in service for ≈13 y at 264°C.
[d] In service for ≈8 y at 284°C.
[e] In service for ≈8 y at 325°C for hot leg and at 291°C for crossover leg, and a hot stand-by for 2.3 y at 303°C for hot leg and at 274°C for crossover leg.

pump cover plate. Results from metallurgical characterization of the various Shippingport materials have been presented earlier.[25]

Microstructural examination indicates that the mechanism of low-temperature embrittlement of the cast materials is the same as that of the laboratory-aged materials.[26,27] All materials showed spinodal decomposition of the ferrite to form a chromium-rich α' phase. In addition, the check-valve materials contained a nickel- and silicon-rich G phase in the ferrite and $M_{23}C_6$ carbides at the austenite/ferrite phase boundary. An unexpected microstructural feature, i.e., σ phase precipitates on slip bands and stacking faults, was also observed in the austenite of the check-valve material. Precipitation of σ phase generally occurs at temperatures >550°C. The presence of σ phase and phase-boundary migration indicate significant differences between the production heat treatment of the check valves and that of the other materials.

The mechanical-property degradation of cast stainless steel (CF-8M) elbows from the Ringhals reactor hot leg and crossover leg was also assessed and compared with experimental data.[28] The chemical composition, ferrite content, and service conditions for the materials are given in Table 2.

3.2 Mechanical Properties

Specimens for Charpy-impact, tensile, and fracture toughness J-R curve tests were obtained from different locations across the thickness of the various components. Baseline mechanical properties for the unaged materials were obtained from either recovery-

Table 3. Values of constants in Eq. 2 for Charpy transition curve of CF-8 cast stainless steels from the Shippingport reactor and KRB pump cover plate

Material ID	Service Condition: Temp., °C	Service Condition: Time, y	Constants: K_0, J/cm²	Constants: B, J/cm²	Constants: C, °C	Constants: D, °C
Cold-Leg Check Valves						
CA4	Annealed	-	25	98.6	-37.0	97.9
CA4	264	13	25	79.2	-20.1	81.8
CB7	264	13	76	108.8	6.0	65.2
Hot-Leg Main Shutoff Valve						
MA9[a]	Annealed	-	96	112.0	-116.3	54.1
MA9	<200	13	83	110.1	-110.7	48.3
MA1/23[a]	Annealed		96	112.0	-116.3	54.1
MA1/23[b]	281	13	73	87.6	-114.2	29.8
MA1/1[c]	281	13	69	63.7	-137.0	38.6
Pump Volutes						
PV	Annealed	-	150	116.2	-151.9	109.7
PV	264	13	75	109.4	-141.9	49.5
VR	Unaged	-	61	88.1	-112.4	38.5
Pump Cover Plate[d]						
KRB	Annealed	-	8	161.9	-16.5	87.2
KRB	284	8	8	119.7	36.8	83.2

[a] Determined from combined data for MA9 and annealed MA9 and MA1.
[b] Material from Rows 2 & 3, which corresponds to 15- to 45-mm region of the wall.
[c] Material from Row 1, which corresponds to inner 15-mm region of the wall.
[d] Obtained from the KRB reactor in Gundremmingen, Germany.

annealed material or material from a cooler region of the component. Microstructural and annealing studies[1,25-27,29] on laboratory- and reactor-aged materials indicate that mechanical properties of unaged material can be determined from recovery-annealed material, i.e., embrittled material that has been annealed for 1 h at 550°C and then water-quenched.

Charpy-impact and tensile data for the various cast materials from the Shippingport reactor have been presented elsewhere.[25] The Charpy data were fitted with the hyperbolic-tangent expression given by

$$C_V = K_0 + B\{1 + \tanh [(T - C)/D]\}, \quad (2)$$

where K_0 is the lower-shelf energy, T is the test temperature in °C, B is half the distance between upper- and lower-shelf energy, C is the mid-shelf Charpy transition temperature (CTT) in °C, and D is the half-width of the transition region. The values of the constants for the various materials are given in Table 3. Examples of the Charpy transition curves for the loop A cold-leg check valve CA4 and pump volute PV are shown in Fig. 5. The results indicate that the room-temperature impact energy of the materials is relatively high and the mid-shelf CTT, i.e., constant C in Eq. 1, is very low. The check valve materials CA4 and CB7 are weaker than MA1 and PV, e.g., the mid-shelf CTT is ≈100°C higher for CA4 and CB7. The higher CTTs are due to the presence of phase-boundary carbides in the check-valve materials. The carbides weaken the phase boundaries and thus provide an easy path for fracture.

The decrease in impact strength from ≈13 y of service at reactor temperatures is minimal for the materials. The room-temperature impact energy of PV, MA1, and CA4 materials is decreased by ≈90, 70, and 40 J/cm², respectively. The large difference in USE for the

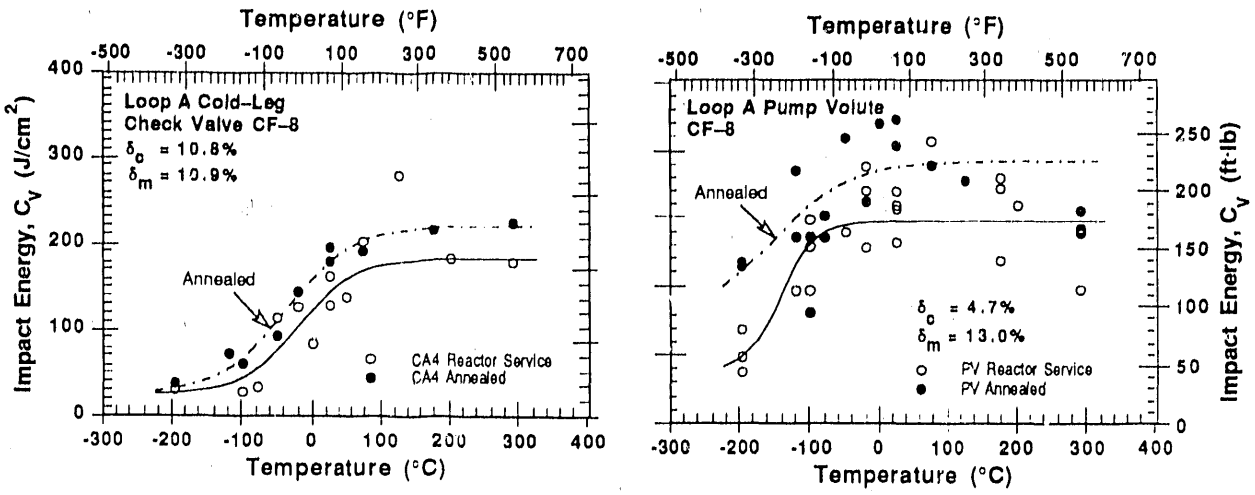

Figure 5. Charpy transition curves for Loop A cold-leg check valve and pump volute after 13 y of service at 264°C. Baseline transition curves represented by results for recovery-annealed material.

unaged and service-aged materials from Row 1 of MA1 (Table 3), is not due to thermal aging. The inner 15-mm region of the MA1 valve body contains a high density of inclusions/ flaws and is inherently weak. The inner surface of all the valves contained repair welds.

Tensile tests were conducted at room temperature and at 290°C on CA4, PV, MA1, and MA9 materials. Tensile properties were also estimated from the instrumented Charpy-impact test data.[25] Examples of the estimated values of yield and ultimate stress, the values obtained from tensile tests, and estimated tensile stresses for recovery-annealed materials from loop A cold-leg check valve CA4 and pump volute PV are shown in Fig. 6.

The estimated tensile properties are in good agreement with the measured values. The tensile strength of CA4, PV, and MA1 materials is comparable. The results show that

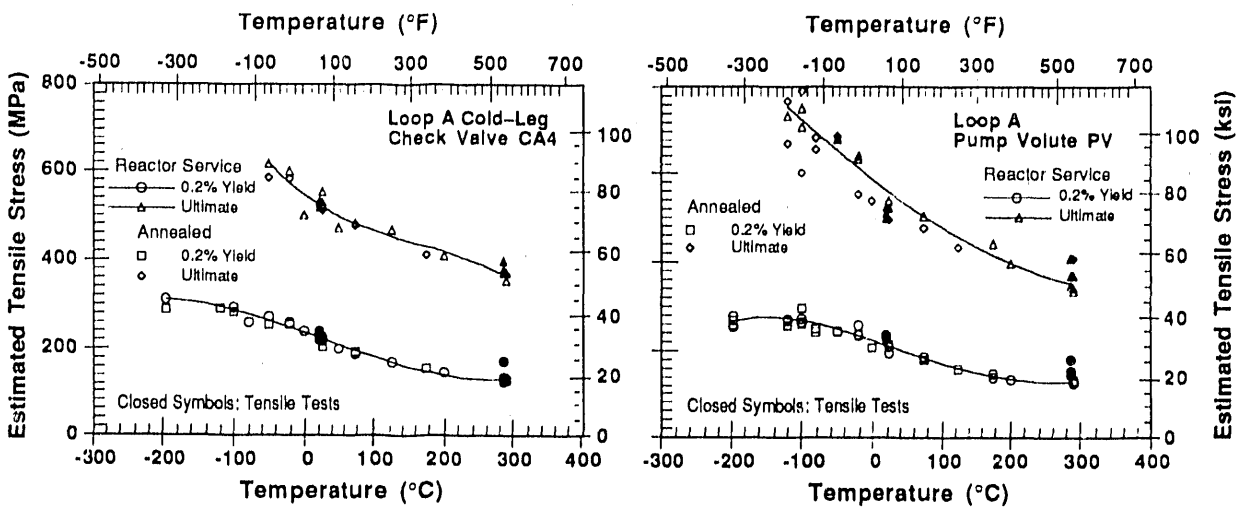

Figure 6. Yield and ultimate stress values (estimated from Charpy-impact data and obtained from tensile tests) for cold-leg check valve and pump volute, and estimated tensile stresses of recovery-annealed materials

thermal aging during reactor service had no effect on yield stress and that the increase in ultimate stress is minimal for all materials. Two specimens of MA1 showed low ultimate strength (and also poor ductility). These specimens were obtained from the inner-15-mm region of the valve body. The poor tensile properties are caused by inclusions in the material. As discussed above, the room-temperature impact energy of Row 1 specimens is also low, e.g., ≈177 ±33 J/cm^2, compared to ≈299 ±33 J/cm^2 for specimens from other regions of the valve body.

3.3 Estimation of Mechanical Properties

Charpy-Impact Energy

A procedure and correlations for predicting mechanical properties of aged cast stainless steels have been described in a companion paper.* Embrittlement of cast stainless steels is characterized in terms of room-temperature Charpy-impact energy. For a specific cast stainless steel, the minimum impact energy that would be achieved for the material after long-term aging (i.e., saturation value) is estimated from Eqs. 1-10 of the companion paper, and the values of room-temperature impact energy as a function of time and temperature of reactor service are estimated from Eqs. 18-22. The information required for the estimations includes the chemical composition, initial impact energy of the unaged material, and the constant θ. A value of 2.9 is assumed for the constant θ in Eqs. 18 and 22 when estimating impact energy of cast stainless steel components in service at 280-330°C. The initial impact energy of the unaged materials was determined from the data for recovery-annealed material or material from a cooler region of the casting. Some materials were aged further in the laboratory at 320, 350, and 400°C to obtain an accurate value of θ and to validate the estimates of the saturation impact energy C_{Vsat} and activation energy for embrittlement of the materials.

The change in estimated Charpy-impact energy with aging time at temperatures between reactor service temperature for the Shippingport and KRB materials and 400°C is shown in Figs. 7-9. The high-temperature aging data for CA4 and MA1 materials represent service-aged material that was aged further in the laboratory. Aging times were adjusted to

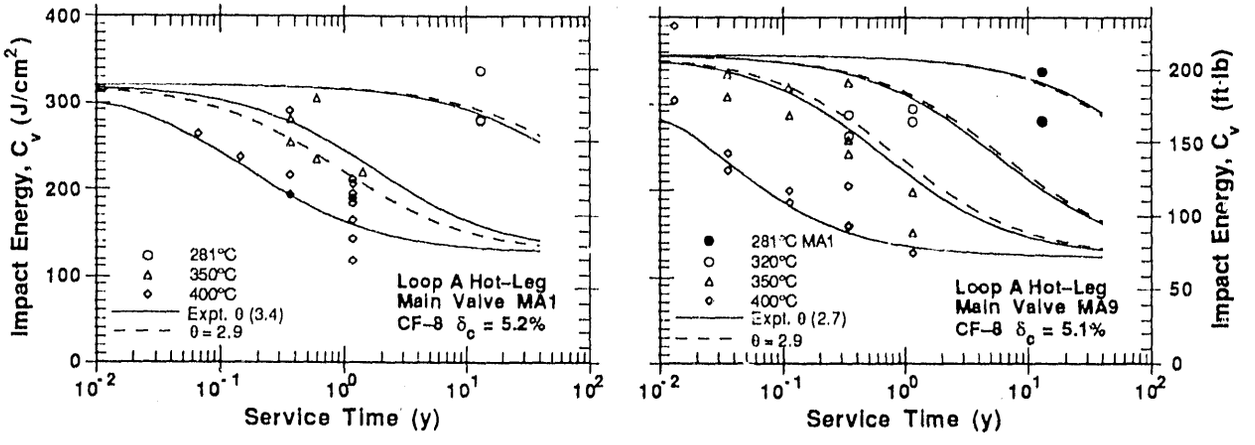

Figure 7. Variation of estimated room-temperature Charpy-impact energy with service time for Loop A hot-leg main valve materials MA1 and MA9. Material MA9 is from a cooler region of the valve. δ_c is calculated ferrite content.

*"Prediction of Aging Degradation of Cast Stainless Steel Components in LWR Systems," this conference.

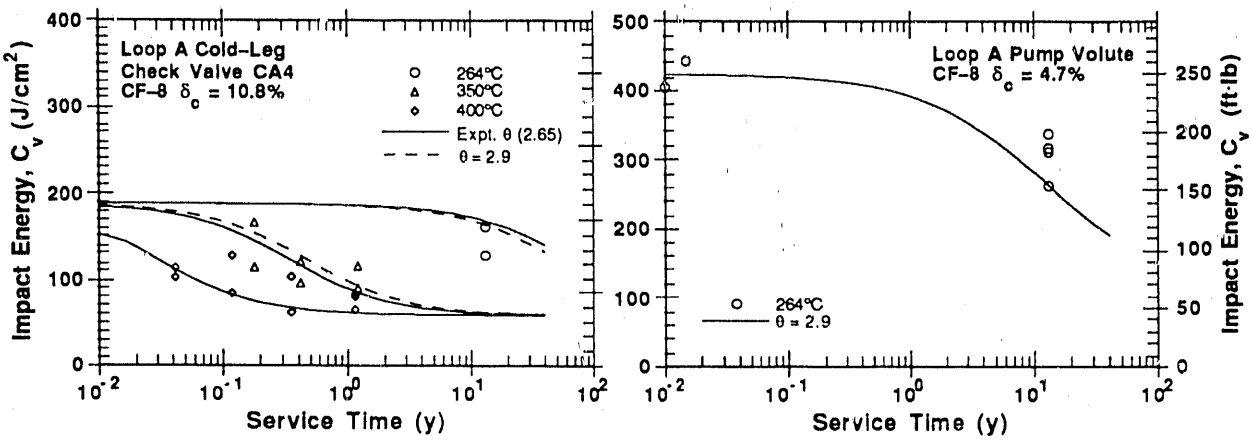

Figure 8. Variations of estimated room-temperature Charpy-impact energy with service time for Loop A cold-leg check valve CA4 and pump volute PV. δ_c is calculated ferrite content.

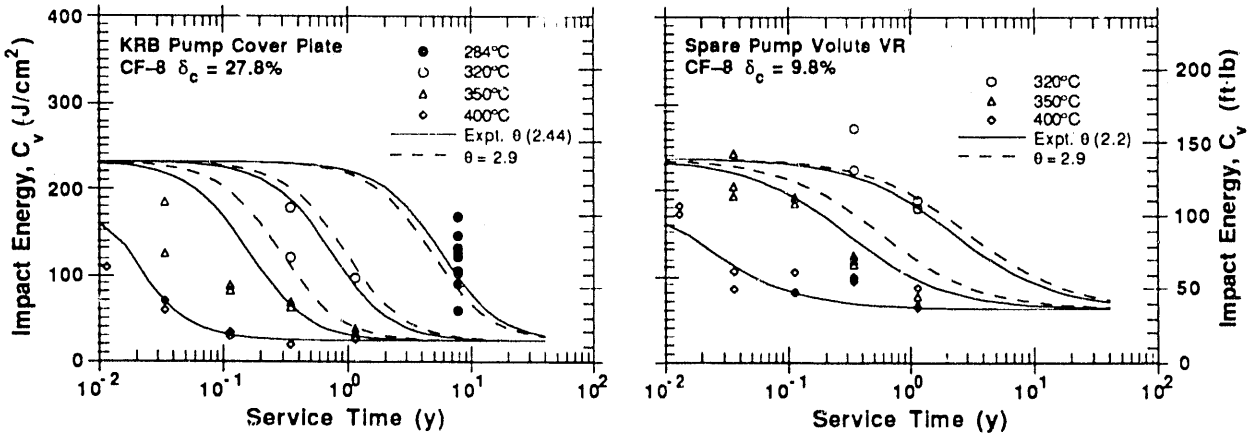

Figure 9. Variations of estimated room-temperature Charpy-impact energy with service time for the KRB pump cover plate and Shippingport spare pump volute VR. .

include the effect of aging at reactor temperature. The high-temperature aging data for the KRB pump cover plate were obtained on recovery-annealed material.

The impact energies estimated with experimental θ show good agreement with the measured impact energies at all temperatures; those estimated with θ = 2.9 show good agreement at temperatures ≤320°C. As mentioned above, estimations based on θ = 2.9 are valid only for service temperatures between 280 and 330°C. For higher temperatures, the estimated values would be nonconservative for materials that have a θ value <2.9, e.g., the KRB pump cover plate and the Shippingport pump volute (Fig. 9). A θ value of 2.5 would give a conservative estimate of impact energy at 330–360°C service temperature.

The impact energy for main valve MA1 was estimated from the compositions of MA1 and MA9 materials; the differences in the compositions of the two materials are minor. Figure 7 shows that, although the aging behavior at 400°C and the kinetics of embrittlement for MA1 and MA9 are significantly different, the estimates based on MA1 and MA9 agree well with the observed values for ≈13 y of service at 281°C. The aging behavior estimated from MA9 is slightly slower than that estimated from MA1.

The predicted minimum saturation room-temperature impact energies also are in very good agreement with the experimental data. The measured impact energies for the VR, MA9, and KRB materials aged at 400°C achieve saturation at the predicted values.

Fracture Toughness

Thermal aging decreases the fracture toughness of cast stainless steels at both room temperature and reactor temperature. The fracture toughness J-R curve for a specific cast stainless steel can be estimated from its room-temperature impact energy C_V (J/cm^2). The J-R curve is expressed by the power-law relation $J_d = C\Delta a^n$, where J_d is deformation J (kJ/m^2) per ASTM Specifications E 813-85 and E 1152-87, Δa is crack extension (mm), and C and n are constants. At room temperature, the J-R curve for static-cast CF-8 steels are estimated from Eqs. 11, 13, and 15 of the companion paper.

The estimated and experimental fracture toughness J-R curves at room temperature and at 290°C for the CA4, MA1, and PV materials and KRB pump cover plate are shown in Figs. 10 and 11. All materials exhibit relatively high fracture toughness. The estimated J-R curves for CA4 and MA1 show good agreement with the experimental results, and those for the PV and KRB materials are 30-50% lower.

Tensile Properties

Thermal aging of cast stainless steels increases their tensile strength, particularly their ultimate stress. The tensile strength of the unaged materials from the Shippingport and KRB reactors was determined from tensile tests or estimated from instrumented Charpy-impact tests on recovery-annealed materials. The materials show slight increases in tensile stress. The increase in flow stress of aged cast stainless steels is estimated from a correlation between the ratio of tensile flow stress of aged, and unaged material and a normalized aging parameter, i.e., Eq. 23 of the companion paper (value of 2.9 for θ was used in the equation). The results, given in Table 4, show good agreement with the measured values.

Fracture toughness J_{IC} values for service-aged materials can be determined from the estimated J-R curve and flow stress, and are also given in Table 4. The estimated J_{IC} shows very good agreement with the measured value for CA4 and is conservative for MA1 and PV.

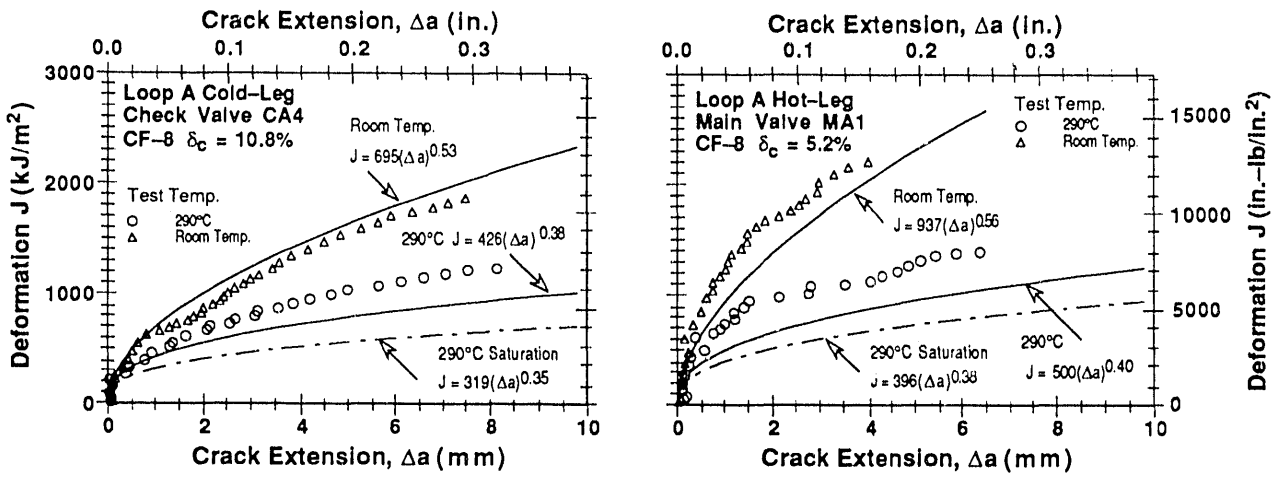

Figure 10. Estimated and measured fracture toughness J-R curve at room temperature and 290°C for the Shippingport cold-leg check valve and hot-leg main valve

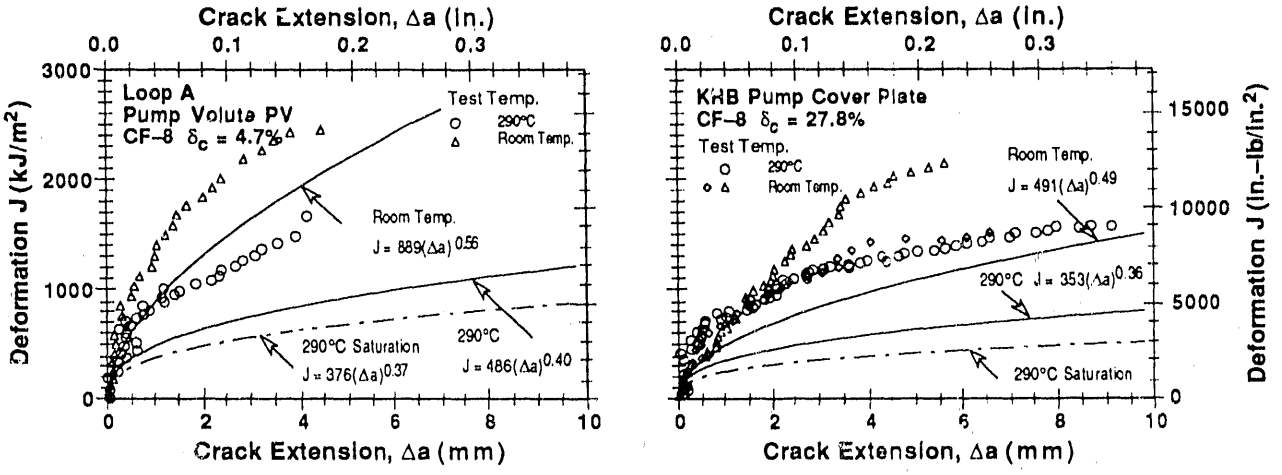

Figure 11. Estimated and measured fracture toughness J-R curve at room temperature and 290°C for the Shippingport cold-leg pump volute and the KRB pump cover plate

Table 4. Measured and estimated tensile flow stress and J_{IC} values for service-aged cast stainless steels

Material ID	Temp., °C	Flow Stress, MPa		J_{IC}, kJ/m^2	
		Observed[a]	Estimated	Observed	Estimated
Shippingport Components					
CA4	25	377 (377)	397	476	485
	290	251 (246)	259	361	331
PV	25	370 (362)	395	1503	692
	290	266 (269)	295	858	373
MA1	25	345 (345)	354	1407	809
	290	237 (233)	238	739	417
KRB Pump Cover Plate					
KRB	25	428 (428)	475	263, 396	297
	290	329 (294)	342	681	249
Ringhals Elbows					
Hot	25	424 (399)	469	250, 330 195, 150	165
	350	315 (292)	362		190
Cross-over	25	392 (369)	409	960, 525 960, 600	247
	350	277 (290)	333		243

[a]Values within parentheses represent unaged material.

4 Thermal Embrittlement of the Ringhals Reactor Elbows

Investigation of the hot- and crossover-leg elbows from the Ringhals reactor indicated significant degradation of impact strength and fracture toughness of the hot-leg elbow after 15 y of service at 325°C, whereas the crossover-leg elbow, in service at 291°C, showed only moderate degradation.[18] The mechanical properties of the Ringhals elbows were estimated from the correlations for CF-8M steel containing >10% Ni. Information on the chemical composition and impact energy of the unaged materials was used in the estimations; θ was assumed to be 2.9.

The experimental data and estimated decrease in impact energy for hot- and crossover-leg elbows during service at 325 and 291°C, respectively, are shown in Fig. 12.

The estimated value of 67 J/cm^2 for the hot-leg elbow is marginally higher than the measured average values of 45 J/cm^2 (equivalent Charpy V-notch impact energy converted from U-notch value) and 50 J/cm^2 (from Charpy V-notch specimens). The estimated 112 J/cm^2 impact energy for the crossover-leg agrees well with 107 J/cm^2 measured from U-notch specimens and is significantly lower than the 177 J/cm^2 obtained from V-notch specimens. The difference between the V- and U-notch impact energy for the crossover-leg elbow is most likely due to a significant variation in the ferrite content of the material. The saturation impact energies for hot- and crossover-leg elbows are estimated to be 56 and 67 J/cm^2, respectively.

Fracture toughness J-R curves can be estimated from the impact energy. Room temperature J-R curve for hot- and crossover-leg elbows after ≈15 y of service are shown in Fig. 15. Only the experimental J_{IC} values (not the complete J-R curve) have been reported for these materials.[28] The estimated tensile flow stress and J_{IC} at room temperature and at 290°C for the Ringhals elbows are given in Table 4. The estimated flow stresses are in good agreement with the measured values. The J_{IC} for the hot-leg elbow also is comparable to the measured value, whereas that for the crossover-leg elbow is 50–70% lower. As mentioned above, the ferrite content of the crossover-leg elbow varies significantly. Furthermore, the correlations do not consider the effect of microstuctural differences and may be conservative for some materials.

5 Conclusions

Characterization of material from the Shippingport NST indicates that the embrittlement of this A212 Grade B steel in a low-temperature, low-flux environment is consistent with the trend band for irradiations at <232°C and shows good agreement with data from test and Army reactors. The shifts in CTT are between 23 and 28°C. The NST weld metal is significantly tougher than the plate material; shift in CTT is ≈20°C. These shifts are significantly lower than those expected on the basis of results obtained from the HFIR surveillance samples. The results indicate that fluence rate does not affect radiation embrittlement at rates as low as 2 x 10^8 n/cm^2·s and at the low operating temperatures of the Shippingport NST, i.e., 55°C. The accelerated embrittlement of HFIR surveillance samples are most likely due to the contribution of thermal neutrons.

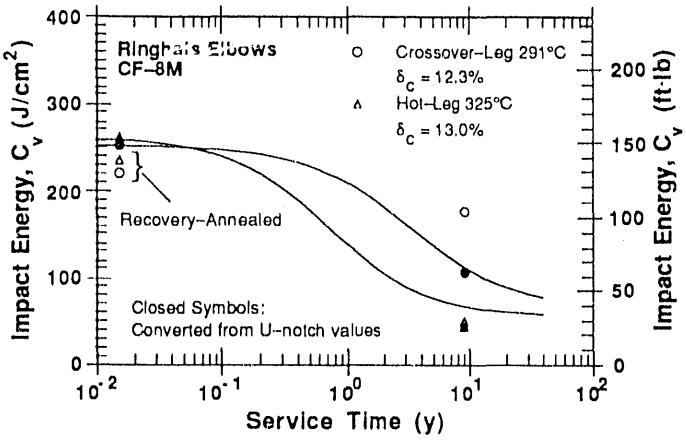

Figure 12.
Estimated and experimentally observed room-temperature Charpy-impact energy for the Ringhals hot- and crossover-leg elbow

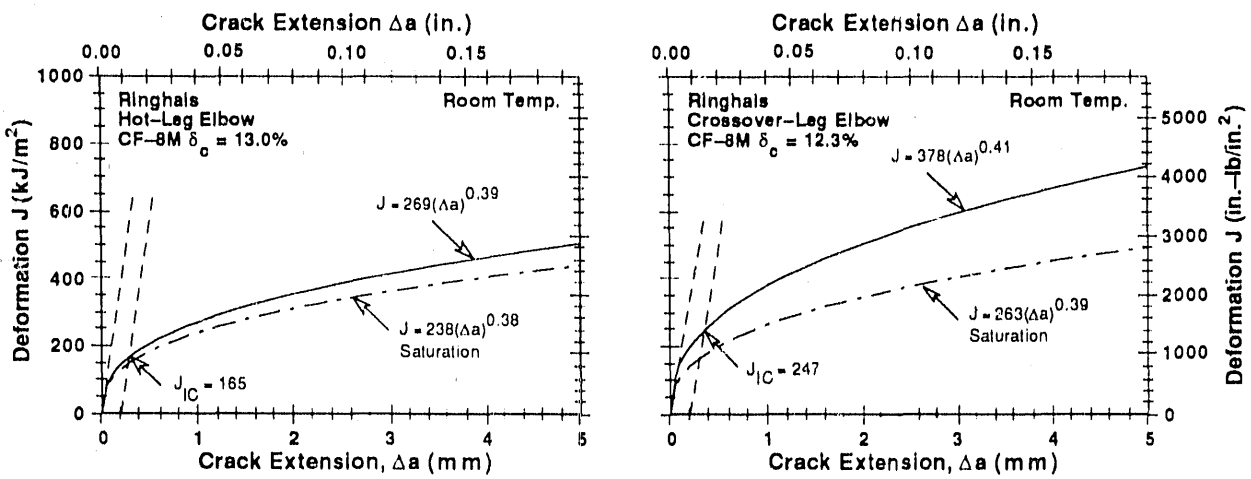

Figure 13. Estimated fracture toughness J-R curve at room temperature for the Ringhals hot- and crossover-leg elbows after ≈13 y of service

Charpy-impact, tensile, and fracture toughness properties of several cast stainless steel materials from the Shippingport, KRB, and Ringhals reactors have been characterized. Baseline mechanical properties for as-cast material were determined from tests on either recovery-annealed material, i.e., material that had been annealed for 1 h at 550°C and then water quenched, or on material from a cooler region of the component. The Shippingport materials exhibited modest degradation of mechanical properties. The room-temperature impact energy was relatively high, >120 J/cm^2 (>70 ft·lb). Check-valve materials were weaker than main valve materials because of the presence of phase-boundary carbides. The CTT for the check valves was ≈100°C higher than that for the main shutoff valves or pump volute. The results show good agreement with estimations based on accelerated laboratory aging studies. The procedure and correlations developed at ANL for estimating thermal aging degradation of cast stainless steels predict accurate or slightly conservative values for Charpy-impact energy, tensile flow stress, fracture toughness J-R curve, and J_{IC} of the Shippingport and KRB materials. The correlations successfully predict the mechanical properties of the Ringhals reactor hot- and crossover-leg elbows after service of ≈15 y.

Acknowledgments

This work was supported by the Office of Nuclear Regulatory Research of the U.S. Nuclear Regulatory Commission. The author thanks A. Sather, T. M. Galvin, L. Y. Bush, W. F. Michaud, and W. F. Burke for experimental contributions and J. Muscara, W. J. Shack, and T. F. Kassner for their helpful discussions.

References

1. R. K. Nanstad, K. Farrell, D. N. Braski, and W. R. Corwin, "Accelerated Neutron Embrittlement of Ferritic Steels at Low Fluence: Flux and Spectrum Effects," *J. Nucl. Mater.*, **158**, 1-6 (1988).
2. R. D. Cheverton, J. G. Merkle, and R. K. Nanstad, *Evaluation of HFIR Pressure Vessel Integrity Considering Radiation Embrittlement*, ORNL/TM-10444, Oak Ridge National Laboratory (April 1988).

3. J. R. Hawthorne, "Studies of Radiation Effects and Pecovery of Notch Ductility of Pressure Vessel Steels," in *Symp. on Steels for Reactor Pressure Circuits*, British Nuclear Energy Conference, Iron and Steel Institute, London, 343–369 (1961).

4. R. D. Cheverton, F. B. Kam, R. K. Nanstad, and G. C. Robinson, "An Embrittlement Rate Effect Deduced from HFIR that May Impact LWR Vessel Support Life Expectancy," *Nucl. Eng. and Des.*, **117**, 349–355 (1989).

5. O. K. Chopra, S. T. Rosinski, and W. J. Shack, "Embrittlement of the Shippingport Reactor Neutron Shield Tank," in *Fatigue, Degradation, and Fracture - 1990*, W. H. Bamford, C. Becht, S. Bhandari, J. D. Gilman, L. A. James, and M. Prager, eds., MPC Vol. 30, PVP Vol. 195, American Society of Mechanical Engineers, New York, pp. 157–168 (1990).

6 O. K. Chopra, W. J. Shack, and S. T. Rosinski, "Radiation Embrittlement of the Neutron Shield Tank from the Shippingport Reactor," NUREG/CR-5748, ANL-91/23, Argonne National Laboratory (July 1991).

7. G. R. Odette, and G. E. Lucas, *Irradiation Embrittlement of LWR Pressure Vessel Steels*, EPRI Report NP-6114, Electric Power Research Institute, Palo Alto, CA (January 1989).

8. G. R. Odette, and G. E. Lucas, "Irradiation Embrittlement of Reactor Pressure Vessel Steels: Mechanisms, Models and Data Correlation," ASTM STP-909, American Society for Testing and Materials, Philadelphia, 206 (1986).

9. R. W. Nichols and D. R. Harries, "Brittle Fracture and Irradiation Effects in Ferritic Pressure Vessel Steels," in *Radiation Effects on Metals and Neutron Dosimetry*, ASTM STP 341, American Society for Testing and Materials, Philadelphia, 162–198 (1963).

10. G. D. Whitman, G. C. Robinson, Jr., and A. W. Savolainen, *Technology of Steel Pressure Vessels for Water-Cooled Nuclear Reactors*, ORNL-NSIC-21, Oak Ridge National Laboratory (December 1967).

11. L. E. Steele and J. R. Hawthorne, "New Information on Neutron Embrittlement and Embrittlement Relief of Reactor Pressure Vessel Steels," in *Flow and Fracture of Metals in Nuclear Environment*, ASTM STP 380, American Society for Testing and Materials, Philadelphia, 283–311 (1965).

12. L. E. Steele and J. R. Hawthorne, "Neutron Embrittlement of Reactor Pressure Vessel Steels," in *Materials and Fuels for High Temperature Nuclear Energy Applications*, The MIT Press, Cambridge, MA, 366–409 (1964).

13. L. E. Steele and C. Z. Serpan, Jr., "Neutron Embrittlement of Pressure Vessel Steels," in *Analysis of Reactor Vessel Radiation Effects Surveillance Programs*, ASTM STP 481, American Society for Testing and Materials, Philadelphia, 49–101 (1966).

14. C. F. Carpenter, N. R. Knopf, and E. S. Byron, "Anomalous Embrittling Effects Observed During Irradiation Studies on Pressure Vessel Steels," *Nucl. Sc. and Eng.*, **19**, 18–38 (1964).

15. J. R. Hawthorne and L. E. Steele, "Metallurgical Variables as Possible Factors Controlling Irradiation Response of Structural Steels," in *Effects of Radiation on Structural Metals*, ASTM STP 426, American Society for Testing and Materials, Philadelphia, 534–572 (1967).

16. J. R. Hawthorne, *Radiation Effects Information Generated on the ASTM Reference Correlation-Monitor Steels*, ASTM Data Series Publication DS-54, American Society for Testing and Materials, Philadelphia (1974).

17. L. E. Steele, J. R. Hawthorne, C. Z. Serpan, Jr., E. P. Klier, and H. E. Watson, *Irradiation Materials Evaluation and Reactor Pressure Vessel Surveillance for the Army Nuclear Power Program*, U.S. Naval Research Laboratory Memorandum Report 1644 (September 1965).

18. L. E. Steele and C. Z. Serpan, Jr., "Army Reactor Vessel Surveillance and Vessel Examination," in *Analysis of Reactor Vessel Radiation Effects Surveillance Programs*, ASTM STP 481, American Society for Testing and Materials, Philadelphia, 105–135 (1966).

19. M. Grounes, "Review of Swedish Work on Irradiation Effects in Pressure Vessel Steels and on Significance of Data Obtained," in *Effects of Radiation on Structural Metals*, ASTM STP 426, American Society for Testing and Materials, Philadelphia, 224–259 (1967).

20. O. K. Chopra and H. M. Chung, "Effect of Low-Temperature Aging on the Mechanical Properties of Cast Stainless Steels," in *Properties of Stainless Steels in Elevated Temperature Service*, M. Prager, ed., MPC Vol. 26, PVP Vol. 132, American Society of Mechanical Engineers, New York, pp. 79–105 (1988).

21. O. K. Chopra, "Thermal Aging of Cast Stainless Steels: Mechanisms and Predictions," in *Fatigue, Degradation, and Fracture – 1990*, W. H. Bamford, C. Becht, S. Bhandari, J. D. Gilman, L. A. James, and M. Prager, eds., MPC Vol. 30, PVP Vol. 195, American Society of Mechanical Engineers, New York, pp. 193-214 (1990).

22. O. K. Chopra and A. Sather, *Initial Assessment of the Mechanisms and Significance of Low-Temperature Embrittlement of Cast Stainless Steels in LWR Systems*, NUREG/CR-5385, ANL-89/17, Argonne National Laboratory, Argonne, IL (August 1990.)

23. O. K. Chopra, *Estimation of Fracture Toughness of Cast Stainless Steels during Thermal Aging in LWR Systems*, NUREG/CR-4513, ANL-90/42, Argonne National Laboratory (June 1991).

24. O. K. Chopra, "Estimation of Mechanical Properties of Cast Stainless Steels during Thermal Aging in LWR Systems," in *Proc. 19th Water Reactor Safety Information Meeting*, U.S. Nuclear Regulatory Commission, (in press, 1992).

25. O. K. Chopra, "Mechanical-Property Degradation of Cast Stainless Steel Components from the Shippingport Reactor," in *Proc. 19th Water Reactor Safety Information Meeting*, U.S. Nuclear Regulatory Commission, (in press, 1992).

26. H. M. Chung, "Thermal Aging of Decommissioned Reactor Cast Stainless Steel Components and Methodology for Life Prediction," in *Life Assessment and Life Extension of Power Plant Components*, T. V. Narayanan, C. B. Bond, J. Sinnappan, A. E. Meligi, M. Prager, T. R. Mager, J. D. Parker, and K. Means, eds., PVP Vol. 171, American Society of Mechanical Engineers, New York, pp. 111–125 (1989).

27. H. M. Chung and T. R. Leax, "Embrittlement of Laboratory and Reactor Aged CF3, CF8, and CF8M Duplex Stainless Steels," *Mater. Sci. and Tech.* **6**, 249–262 (1990).

28. C. Jansson, "Degradation of Cast Stainless Steel Elbows after 15 Years in Service," presented at *Fontevraud II Intl. Symp.*, Sept. 10–14, 1990, Royal Abbey of Fontevraud, France.

29. H. M. Chung and O. K. Chopra, "Long-Term-Aging Embrittlement of Cast Austenitic Stainless Steels – Mechanism and Kinetics," in *Properties of Stainless Steels in Elevated Temperature Service*, M. Prager, ed., MPC Vol. 26, PVP Vol. 132, American Society of Mechanical Engineers, New York, pp. 17–34 (1988).

DATE
FILMED
8103192